Contrast enhancement by differently sized paramagnetic MRI contrast agents in mice with two phenotypes of atherosclerotic plaque

CONTRAST MEDIA & MOLECULAR IMAGING

Received: 12 January 2010, Revised: 27 April 2010, Accepted: 29 May 2010, Published online in Wiley Online Library: 29 September 2010

(wileyonlinelibrary.com) DOI:10.1002/cmmi.402

Contrast enhancement by differently sized paramagnetic MRI contrast agents in mice with two phenotypes of atherosclerotic plaque

Glenda S. van Bochove[a], Leonie E.M. Paulis[a], Dolf Segers[b], Willem J.M. Mulder[c], Rob Krams[d], Klaas Nicolay[a] and Gustav J. Strijkers[a]*

Interest in the use of contrast-enhanced MRI to enable *in vivo* specific characterization of atherosclerotic plaques is increasing. In this study the intrinsic ability of three differently sized gadolinium-based contrast agents to permeate different mouse plaque phenotypes was evaluated with MRI. A tapered cast was implanted around the right carotid artery of apoE$^{-/-}$ mice to induce two different plaque phenotypes: a thin cap fibroatheroma (TCFA) and a non-TCFA lesion. Both plaques were allowed to develop over 6 and 9 weeks, leading to an intermediate and advanced lesion, respectively. Signal enhancement in the carotid artery wall, following intravenous injection of Gd-HP-DO3A as well as paramagnetic micelles and liposomes was evaluated. *In vivo* T_1-weighted MRI plaque enhancement characteristics were complemented by fluorescence microscopy and correlated to lesion phenotype. The two smallest contrast agents, i.e. Gd-HP-DO3A and micelles, were found to enhance contrast in T_1-weighted MR images of all investigated plaque phenotypes. Maximum contrast enhancement ranged between 53 and 70% at 6 min after injection of Gd-HP-DO3A with highest enhancement and longest retention in the non-TCFA lesion. Twenty-four hours after injection of micelles maximum contrast enhancement ranged between 24 and 35% in all plaque phenotypes. Administration of the larger liposomes did not cause significant contrast enhancement in the atherosclerotic plaques. Confocal fluorescence microscopy confirmed the MRI-based differences in plaque permeation between micelles and liposomes. Plaque permeation of contrast agents was strongly dependent on size. Our results implicate that, when equipped with targeting ligands, liposomes are most suitable for the imaging of plaque-associated endothelial markers due to low background enhancement, whereas micelles, which accumulate extravascularly on a long timescale, are suited for imaging of less abundant markers inside plaques. Low molecular weight compounds may be employed for target-specific imaging of highly abundant extravascular plaque-associated targets. Copyright © 2010 John Wiley & Sons, Ltd.

Keywords: atherosclerosis; MRI; Gd-HP-DO3A; micelle; liposome

1. INTRODUCTION

Blood flow-induced shear stress on the vascular endothelium plays a critical role in the onset and development of atherosclerosis. Plaque formation has been shown to occur mostly in low shear stress areas such as the inner curvatures of coronary arteries, or near bifurcations where shear stress is low and oscillatory (1). Vascular segments with laminar flow and higher shear stress are less likely to develop atherosclerosis. Cheng *et al*. identified shear stress patterns as essential factors in the development, as well as in the size, and composition of atherosclerotic lesions (2). Their studies in apoE$^{-/-}$ mice on a lipid-rich diet revealed that a tapered cast, placed around the carotid artery, induces two different lesion phenotypes on either side of the cast. Upstream of the cast, due to lowered shear stress, a lesion with characteristics of a thin cap fibroatheroma [TCFA (3)] was formed, i.e. distinguished by high lipid content and lower collagen and smooth muscle cell content. Downstream of the cast, as a consequence of oscillatory shear stress, a fibrous plaque with stable characteristics was formed.

MRI has proven to be excellently suited for non-invasive high-resolution imaging of the vessel lumen and vessel wall, in particular of the larger blood vessels (4–8). Using a combination

* *Correspondence to: G. J. Strijkers, Biomedical NMR, Department of Biomedical Engineering, Eindhoven University of Technology, PO Box 513, 5600 MB Eindhoven, The Netherlands.*
E-mail: g.j.strijkers@tue.nl

a *G.S. van Bochove, L.E.M. Paulis, K. Nicolay, G.J Strijkers*
Biomedical NMR, Department of Biomedical Engineering, Eindhoven University of Technology, Eindhoven, The Netherlands

b *D. Segers*
Department of Cardiology, Erasmus MC, Rotterdam, The Netherlands

c *W.J.M. Mulder*
Translational and Molecular Imaging Institute, Mount Sinai School of Medicine New York, NY, USA

d *R. Krams*
Department of Bioengineering, London Imperial College, London, United Kingdom

of different protocols such as T_1-weighted, T_2-weighted, PD-weighted and diffusion-weighted sequences, MRI provides a basic analysis of the major plaque components (9).

Apart from these 'traditional' MR imaging approaches, there is increasing interest in the use of MR contrast agents that enable a more refined characterization of atherosclerotic plaques (10). Dynamic contrast-enhanced imaging using gadolinium-based contrast agents such as gadofluorine (11,12) and gadodiamide (13) has been explored to investigate plaque neo-vascularization and permeability. Injection of USPIOs enabled the detection of plaque-associated macrophages in animal models (14,15) as well as in humans (16). Target-specific contrast agents have been applied for imaging of a range of plaque features, such as vascular adhesion molecule-1 expression (17), macrophage burden (18,19), angiogenic activity (20,21) and thrombus formation (22,23).

Although the above studies have demonstrated that imaging of specific plaque processes is feasible, differentiation between TCFA and fibrous plaques on the basis of target-specific MR imaging has not been demonstrated thus far. The introduction of the above-mentioned mouse model (24) opens up the possibility to investigate different plaque phenotypes within a single vascular segment, which allows rigorous studies with contrast agents that aim to discriminate plaque phenotypes.

However, the discrimination between lesion phenotypes using targeted contrast agents assumes differences in non-specific accumulation to be absent in the TCFA and non-TCFA regions. Contrast agent permeation into plaques is likely to be dependent on many factors, including particle properties (size, charge, 3D configuration, lipophilicity) as well as the local plaque environment (wall shear stress, endothelial permeability, presence of phagocytic cells). It is thus valuable to investigate the differences in accumulation of contrast agents in the two shear stress regions as a function of particle size. Therefore the goal of this study was to characterize the plaques in this mouse model of atherosclerosis at two developmental stages using MRI and to investigate plaque permeation of three differently sized gadolinium-based contrast agents.

To that aim we evaluated signal enhancement in plaques after intravenous administration of Gd-HP-DO3A as well as gadolinium-containing micelles (~15 nm) and liposomes (~125 nm). *In vivo* T_1-weighted MRI enhancement characteristics were complemented by fluorescence microscopy and correlated to lesion phenotype as assessed by immunohistology.

2. RESULTS AND DISCUSSION

2.1. Plaque phenotype

Histological evaluation confirmed subtle differences in plaque composition of the lesions upstream and downstream of the cast. An exhaustive characterization of the plaque phenotype was performed previously by Cheng *et al.* (2). Here we restrict ourselves to a description of the basic histological features, which are summarized in Table 1. On basis of these features and previous characterization (2,25) upstream lesions will be referred to as 'TCFA' and the downstream lesions as 'non-TCFA'. Briefly, all plaques were rich in lipids (Fig. 1E–H), with the non-TCFA plaques displaying fewer droplets of lipids while the TCFA plaques displayed a necrotic core.

Plaques developed over 9 weeks were larger in longitudinal direction and the above difference in lipid content between the two plaque types was more pronounced than for plaques developed over 6 weeks. Macrophages were present at similar amounts in the TCFA and non-TCFA plaques, at both developmental stages of the lesions. A cap of smooth muscle cells was most evident after 9 weeks. In the TCFA plaque at both developmental stages, only a little collagen was present, consistent with a more vulnerable phenotype. In the non-TCFA plaque after 6 weeks collagen fibers were seen throughout the entire plaque (Fig. 1R). In the 9 weeks non-TCFA plaque, thicker collagen rich regions were also found (Fig. 1T). In general, more pronounced differences in plaque phenotypes were found in the 9 weeks lesions as compared with the 6 weeks lesions. Based on these histology classifications we will refer to the 6 weeks lesion as 'intermediate' and the 9 weeks lesion as 'advanced', in the remainder of this paper.

2.2. Size and relaxivities of the different contrast agents

The basic characterization of the paramagnetic agents involved measurements of their size and, for their MR-performance, the relaxivity at 1.41 T (in the range of clinical field strengths) and 6.3 T (field strength preclinical MRI scanner used for this study), as shown in Table 2.

At a mean diameter of 16 nm, micelles were a factor of 7–8 smaller than liposomes, but displayed the highest relaxivity. A lower relaxivity (both r_1 and r_2) at 6.3 T compared with 1.41 T was observed for liposomes and micelles, while for Gd-HP-DO3A

Table 1. Histological classification of plaque phenotype

	6 weeks		9 weeks	
	Upstream	Downstream	Upstream	Downstream
Macrophages	+	+	+	+
Lipids	++	+	++	+
Smooth muscle cells	−	—	−	—
Collagen	−	+	−	++
Classification	TCFA	non-TCFA	TCFA	non-TCFA
	intermediate		advanced	

Explanation of symbols: — = lowest; − = low; + = high; ++ = highest.

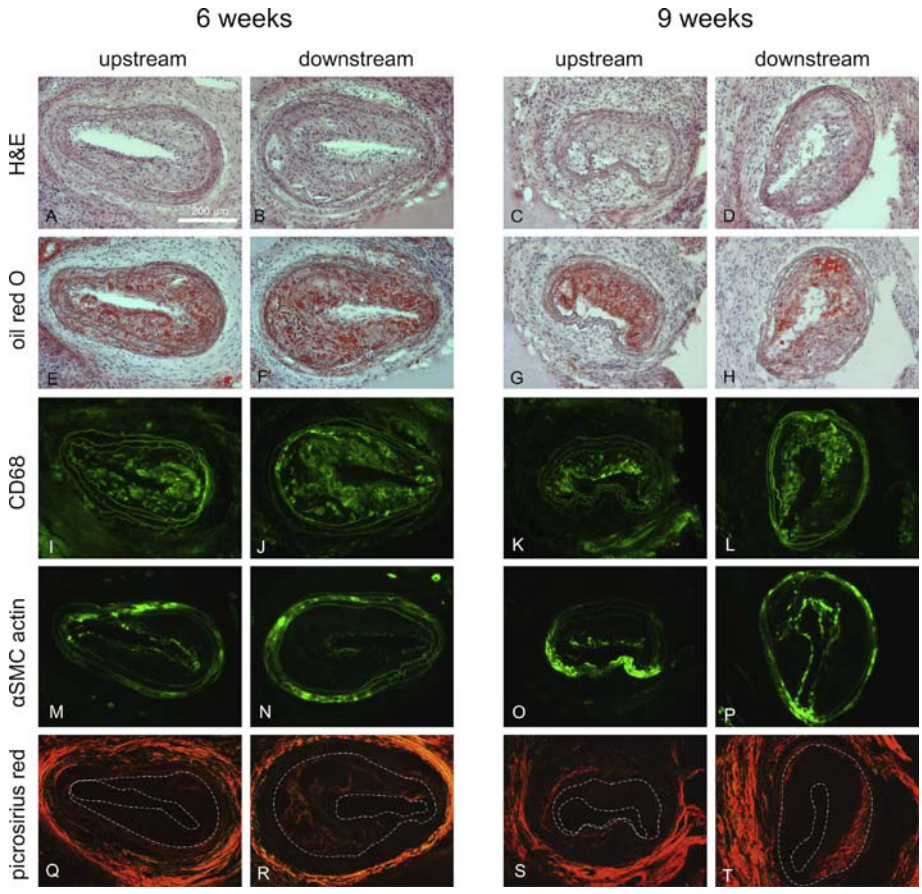

Figure 1. Sections of right carotid arteries 6 and 9 weeks after cast placement, which were stained with hematoxylin and eosin (H&E), Oil red O for lipids, anti-CD68-FITC for macrophages, anti-α-smooth muscle actin-FITC for smooth muscle cells and picrosirius red for collagen. The dashed lines in the picrosirius red staining indicate the plaque borders. Based on histology, plaques are classified as: 6 weeks = intermediate, 9 weeks = advanced, upstream = 'TCFA', downstream = 'non-TCFA'.

slightly higher values were found at the higher field-strength. The latter result is probably caused by the temperature difference between the measurements at the different field strengths.

2.3. Blood circulation half-lives and bio-distribution

Knowledge of blood clearance rates and bio-distribution is critical for understanding contrast agent behavior. As depicted in Fig. 2A, blood circulation half-lives amounted to 7.0 ± 1.0 h ($R^2 = 0.94$) for liposomes, 22.5 ± 2.8 h ($R^2 = 0.93$) for micelles and 7.9 ± 3.0 min ($R^2 = 0.73$) for Gd-HP-DO3A. As expected, at 48 h after injection of liposomes and micelles, the highest gadolinium content was found in the liver and spleen (Fig. 2B). Gadolinium levels of the liver corresponded to approximately 50 and 35% of the total injected dose for liposomes and micelles, respectively. For the spleen, these values were approximately 1 and 3%. Negligible amounts of gadolinium were found in the lungs, while a small amount was found in the kidneys ($\sim$7 μg/g tissue). At 48 h, Gd-HP-DO3A was found mostly in the kidneys (28 μg/g tissue, approximately 8% of the total injected dose).

2.4. MR Angiography

MR imaging sessions routinely began with MR angiography (Fig. 3A) to confirm flow preservation through the right carotid artery and to precisely localize the position of the cast with

Table 2. Size distributions and relaxivities of the different contrast agents

Contrast agent	Hydrodynamic diameter (nm)	r_1, 1.41 T, 37°C ($mM^{-1}s^{-1}$)	r_2, 1.41 T, 37°C ($mM^{-1}s^{-1}$)	r_1, 6.3 T, room temperature ($mM^{-1}s^{-1}$)	r_2, 6.3 T, room temperature ($mM^{-1}s^{-1}$)
Liposomes	123 ± 5	6.8	9.6	2.5	6.4
Micelles	16 ± 1	11.8	17.8	4.5	13.0
Gd-HP-DO3A	-	3.3	4.0	4.2	4.5

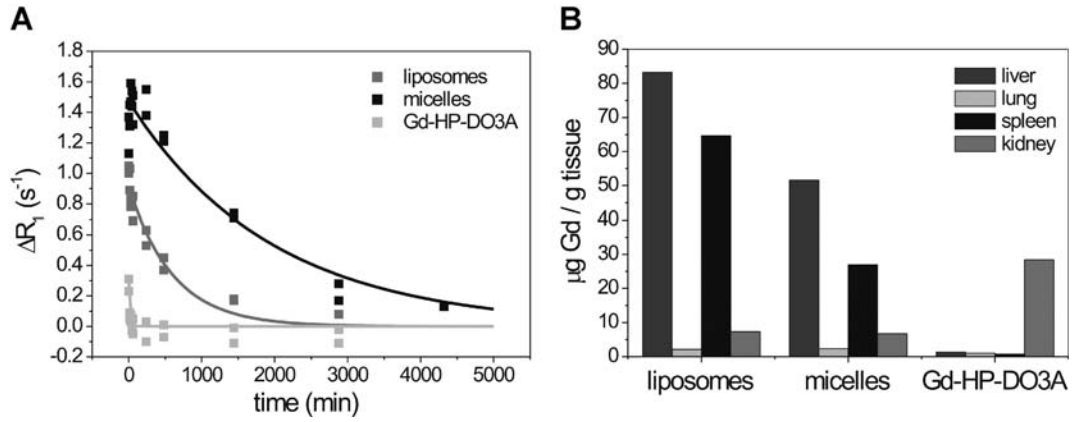

Figure 2. (A) ΔR_1 of blood samples after injection of liposomes, micelles and Gd-HP-DO3A ($n = 2$ for each contrast agent). Solid lines are mono-exponential fittings of ΔR_1 values as a function of time [$t_{1/2}$ of liposomes $= 7.0 \pm 1.0$ h ($R^2 = 0.94$), $t_{1/2}$ of micelles $= 22.5 \pm 2.8$ h ($R^2 = 0.93$), $t_{1/2}$ of Gd-HP-DO3A $= 7.9 \pm 3.0$ min ($R^2 = 0.73$)]. (B) Gadolinium content (µg/g tissue) in liver, lung, spleen and kidney 48 h after contrast agent injection as determined by ICP-AES and ICP-MS ($n = 1$ for each contrast agent).

respect to the arterial tree. A signal void was observed at the location of the cast, which was used to position slices for T_1-weighted imaging perpendicular to the carotid artery directly upstream and downstream to the cast. Angiography performed 1.5 h after administration of paramagnetic liposomes and micelles revealed the smaller arteries and larger veins as well (Fig. 3B). This observation confirmed successful tail-vein injection of contrast agent.

2.5. Sagittal and axial imaging

Sagittal imaging revealed the right carotid artery and the location of the cast (Fig. 3C). In these images narrowing of the vessel lumen was seen due to plaque formation on both sides of the cast. An axial image upstream of the cast made before contrast agent injection is shown in Fig. 3D. In most cases right carotid artery wall signal intensities were higher than surround-

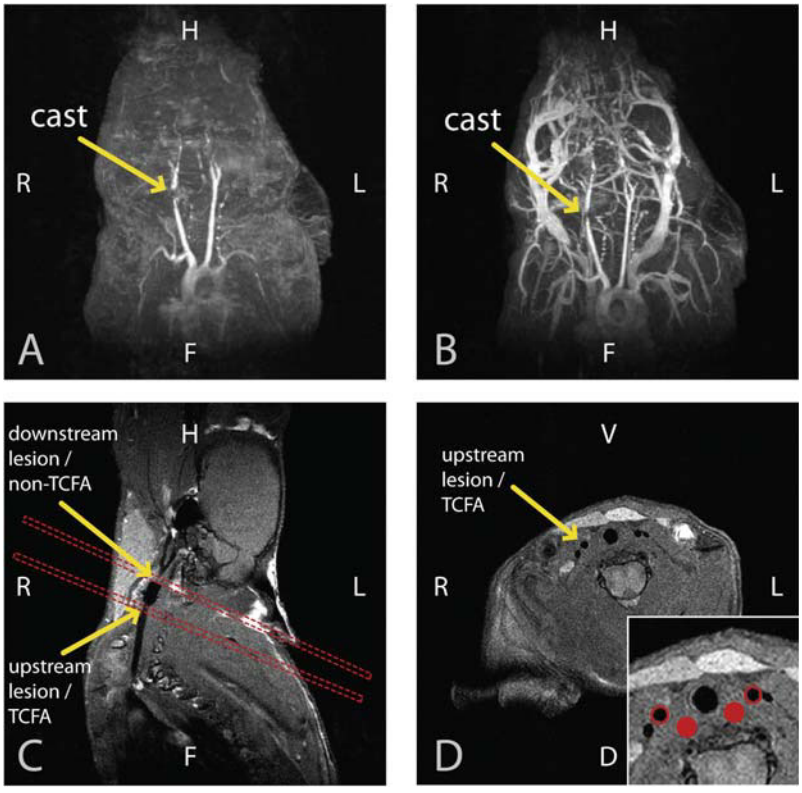

Figure 3. Maximum intensity projections of 3D TOF angiography of the neck region of a mouse before (A) and 1.5 h after (B) liposome injection. The position of the cast around the carotid artery is indicated by the arrows in A and B. Sagittal (C) and axial (D) T_1-weighted images of the neck region of the mouse as collected before contrast agent injection. The axial image was made upstream of the cast. The inset shows the placement of two ROIs in the wall of both carotid artery vessels and two ROIS in the surrounding muscle (H = head, F = feet, V = ventral, D = dorsal, L = left, R = right).

ing muscle due to the presence of a lesion, which facilitated accurate positioning of the regions of interest (ROIs) on the vessel wall lesion for quantitative image analysis (inset of Fig. 3D). The MRI signal from the non-lesioned artery wall was essentially isointense with muscle.

2.6. T_1-weighted imaging

Figure 4 shows a collection of MR images of all different lesion types investigated, pre- and post-contrast agent injection of liposomes, micelles and Gd-HP-DO3A. T_1-weighted MR imaging (Fig. 4A) did not show evidence of contrast enhancement by liposomes in TCFA and non-TCFA lesions at both intermediate and advanced stages of development. Injection of micelles (Fig. 4B) did lead to visible, typically non-uniform, contrast enhancement for both plaque phenotypes after 24 h. Contrast enhancement was already observed as early as 15 min after injection of paramagnetic micelles in two out of six mice. Gd-HP-DO3A caused maximum contrast enhancement at the first timepoint, i.e. 3.5 min after injection. Subsequently, the contrast enhancement decreased and was no longer visible after 1 h (Fig. 4C).

2.7. Temporal contrast behavior

Even though plaque dimensions were not quantified, we infer that the analyzed images did not suffer from partial volume effects in the vessel direction, since in most cases plaque enhancement was observed in directly neighboring imaging slices. Injection of liposomes only led to a significantly increased percentage of normalized signal enhancement (%NSE) in the advanced TCFA lesions 15 min after injection (Fig. 5A, B). Both TCFA and non-TCFA plaques were significantly enhanced 24 h after micelle administration at both intermediate and advanced stages (Fig. 5C, D). The micelle-induced enhancements of the intermediate TCFA plaque and the advanced non-TCFA plaque were also significantly different from both liposomes and Gd-HP-DO3A after 24 h. The average enhancement 24 h after micelle injection ranged from 23.7 to 34.6%. For Gd-HP-DO3A enhancement occurred for all vessel wall segments after 15 min (Fig. 5E and F) with enhancements ranging from 12.0 to 18.0% in the left carotid artery and from 29.7 to 36.7% in plaques. At this timepoint enhancement in both plaque phenotypes was also different from liposomes and micelles, except for liposomes in the advanced vulnerable plaque. It should be noted that the non-TCFA plaque exhibited the largest Gd-HP-DO3A-induced enhancement (31.1–36.7%) in all cases, followed by the TCFA plaque (23.5– 29.7%). The left carotid artery always showed the smallest enhancement. However, differences in %NSE between non-TCFA and TCFA plaques did not reach significance in any of the cases.

2.8. High temporal resolution contrast behavior of Gd-HP-DO3A

Figure 5G, H shows the percentage signal enhancement (%SE) for the Gd-HP-DO3A group at higher temporal resolution up to 60 min after injection. The first timepoint after contrast injection showed the highest contrast enhancement (53.4–69.5% in plaques and 28.7–31.1% in the left carotid artery). A mono-exponential decay function was used to estimate the half-life of enhancement for each plaque phenotype. Half-lives were found to be 15.3 ± 0.5 min ($R^2 = 0.996$) for the intermediate TCFA plaque in the right carotid artery, 20.1 ± 1.2 min ($R^2 = 0.982$) for the intermediate non-TCFA plaque and 18.9 ± 2.2 min ($R^2 = 0.941$) in

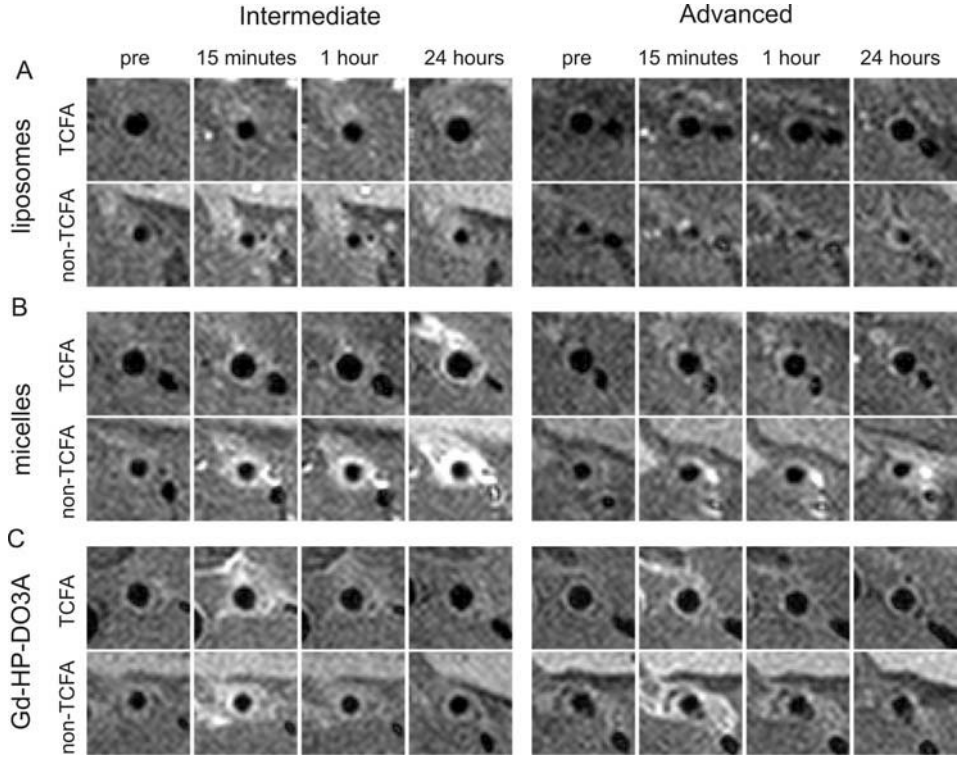

Figure 4. Representative axial T_1-weighted images of the right carotid artery for each group, as collected before and after contrast agent injection. The original images were cropped to select the right carotid artery (FOV 0.25×0.25 cm^2).

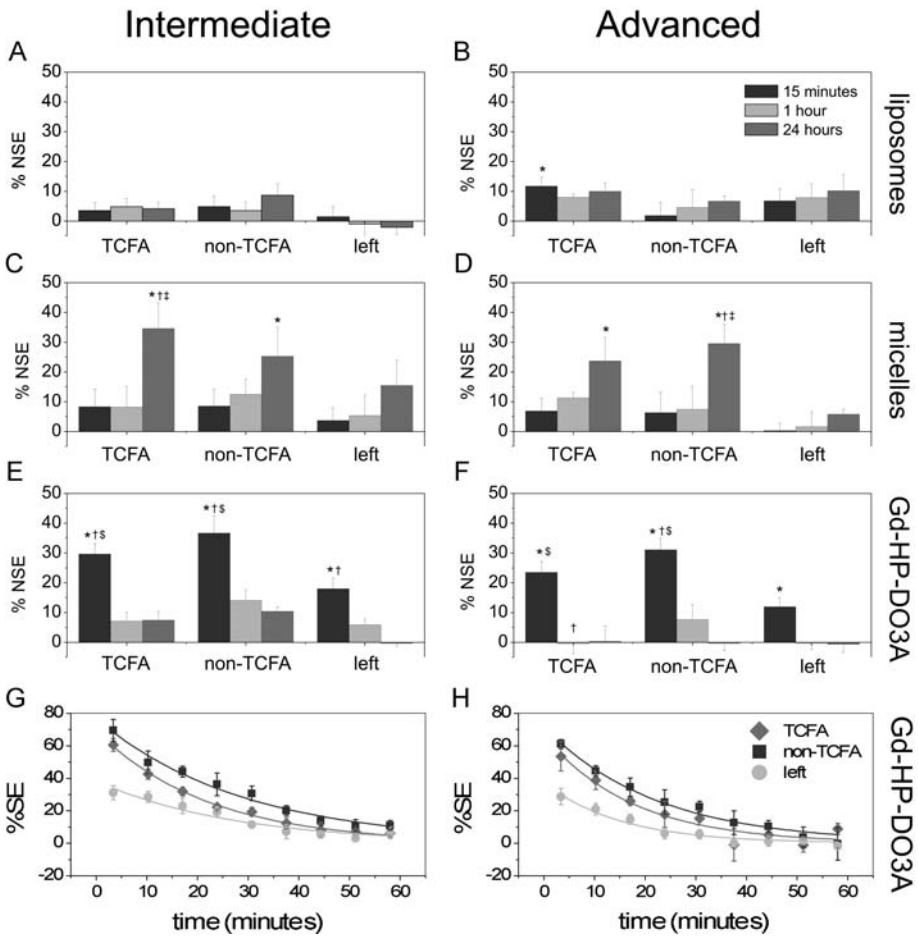

Figure 5. Percentage normalized signal enhancement (%NSE, mean ± SEM) over time as measured in the upstream TCFA plaque, the downstream non-TCFA plaque and the left carotid artery as a control, after injection of liposomes (A, B), micelles (C, D) and Gd-HP-DO3A (E, F), in the intermediate (A, C, E) and advanced (B, D, F) stage of plaque development (G, H). The percentage signal enhancement (%SE, mean ± SEM) of the vessel wall over time for the mice injected with Gd-HP-DO3A in the intermediate (G) and advanced (H) stages. Significantly different from pre (*); liposomes (†); micelles ($); and Gd-HP-DO3A (‡), Bonferroni 95%.

the vessel wall of the left carotid artery. Values of 12.1 ± 1.6 min ($R^2 = 0.941$) in the advanced TCFA lesion, 15.4 ± 1.1 min ($R^2 = 0.979$) in the advanced non-TCFA lesion and 10.4 ± 1.2 min ($R^2 = 0.963$) in the corresponding left vessel wall were found. At both intermediate and advanced stages, %SE in the TCFA plaque, non-TCFA plaque and left vessel wall ROIs were significantly different from each other (multifactor ANOVA, $p < 0.001$). The non-TCFA plaque showed initially highest and longest retention of contrast enhancement after Gd-HP-DO3A injections as compared with the TCFA plaque.

2.9. Detection of MRI-contrast agent with confocal laser scanning microscopy

Carotid artery specimens were obtained 24 h after contrast agent injection. Confocal laser scanning microscopy of plaques from animals injected with paramagnetic, fluorescent liposomes did not convincingly reveal fluorescent signal from liposomes (Fig. 6A–D). In some cases, diffuse fluorescence was observed in the adventitia (Fig. 6B) and on occasion weakly in the plaque (Fig. 6D). Fluorescence from micelles, however, was observed throughout the entire plaque in sections of the advanced lesions (Fig. 6G, H) as well as in the smaller plaques of the intermediate lesions (Fig. 6E, F). In the adventitia, the incidentally found fluorescence of micelles was much weaker than in the plaques. As Gd-HP-DO3A has no fluorescent label, material from animals injected with this agent served as a control for confocal laser scanning microscopy to show the absence of autofluorescent background signal. Representative images are shown Fig. 6I–L. As expected, no fluorescence was detected. The lack of differences in contrast agent accumulation characteristics in TCFA and non-TCFA plaques, justifies the future use of lipid-based contrast agents targeted towards specific plaque constituent with the purpose of discriminating the stable and vulnerable plaque phenotypes.

2.10. Liposomes

The liposomes were relatively large (~125 nm), which most likely explains the prevention of accumulation in all lesions of this mouse model. Liposomes have a high relaxivity, contain many gadolinium moieties per particle and have a long circulation half-life. The absence of intraplaque accumulation as found in the current study becomes an advantage when considering certain forms of targeted imaging. When these liposomes are equipped with targeting moieties they are best suited for targeting of

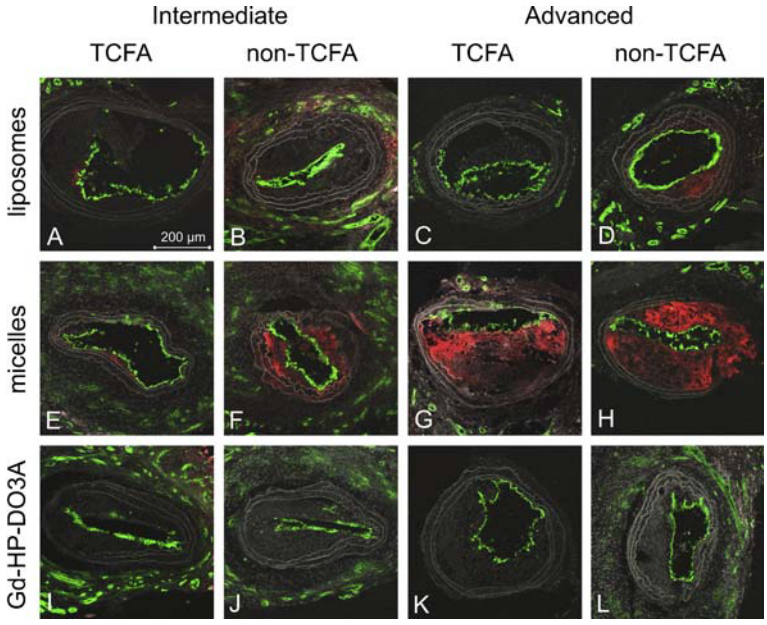

Figure 6. Confocal laser scanning microscopy of right carotid artery specimens from mice injected with liposomes (top row, A–D), micelles (middle row, E–H) and Gd-HP-DO3A (bottom row, I–L). The intermediate lesions are shown in the left two colums (A, B, E, F, I, J) and the advanced lesions in the two right columns (C, D, G, H, K, L). TCFA lesions are shown on position A, E, I, C, G and K. Non-TCFA lesions are shown on position B, F, J, D, H and L. In green: endothelial cells (CD31); red: contrast agent (NIR664-DSPE); grayscale background: autofluorescence for anatomical reference.

endothelial markers available from the lumen. Mulder *et al.* (24) did find contrast enhancement in the carotid artery of apoE$^{-/-}$ mice upon administration of similar liposomes. In the latter study, mice were measured 2 weeks after placement of a restrictive collar (26) around the carotid artery, which resulted in the formation of a more advanced lesion.

2.11. Micelles

Micelles were found to accumulate in both plaque phenotypes with comparable MRI signal enhancements (25–30%) 24 h post-injection. Some non-TCFA plaques already enhanced within 1 h. The close vicinity of the carotid artery bifurcation to the non-TCFA plaque could have affected flow patterns at this location, leading to an earlier uptake of micelles as compared with the TCFA plaque. We were not able to confirm such variation using histology. Since micelles are able to penetrate plaques, they seem excellently suited to target intraplaque constituents. However, the site-dependency of the passive accumulation of micelles must be carefully considered. Targeted micelles have already been used in several studies to visualize intraplaque markers (19,27,28). Attaching ligands to nanoparticles may cause a considerable increase in their size. We therefore advocate the use of micelles equipped with non-binding antibodies or scrambled peptides as controls for targeted micelles instead of non-conjugated micelles to rule out size-related differences in distribution patterns. Moreover, differences in blood clearance kinetics between different agents should be carefully considered.

In our study an animal model was employed in which two phenotypically different plaques develop in the same arterial segment. Equal levels of contrast enhancement in both plaques were found after accumulation of micelles for 24 h. This justifies the comparison of enhancement levels between these two phenotypes when applying targeted contrast agents. However, within the first hour after injection of micelles the non-TCFA plaque showed large variation in contrast enhancement behavior, which will make straightforward comparison between targeted and control agents at these timepoints more difficult. For the future use of micelles to target intraplaque constituents, there are still application barriers that need to be overcome. Notably, non-specific enhancement, i.e. due to accumulation, slow-washout and phagocytosis, could lower the effective target-to-background ratio and thus specificity of the targeted micelles. We believe therefore that measurements and modeling of the wash-in and wash-out kinetics of the contrast agents will prove essential for successful application of these contrast agents targeted to intraplaque consituents.

2.12. Gd-HP-DO3A

Images made after injection of Gd-HP-DO3A showed that this contrast agent diffuses easily into the vessel wall and is already washed out after approximately 1 h. The left carotid artery as control showed a much lower enhancement as compared with plaques and, in addition, exhibited varying retention patterns. However, the presence of plaque in the left carotid artery cannot be fully excluded. In all cases, the initial vessel wall enhancement and the estimated signal enhancement half-life was larger for the non-TCFA plaque than for the TCFA plaque, indicating a more extensive accumulation of Gd-HP-DO3A in the stable lesion. Even though this difference was rather subtle, higher contrast enhancement of more fibrous lesions was previously also found in other studies with low molecular weight contrast agents. Yuan *et al.* (29) and Wasserman *et al.* (30) showed minimal entry in lipid-rich necrotic regions and highest levels of contrast enhancement in fibrous tissue in plaques in patients. Kerwin *et al.* (13) observed a range in plaque enhancement patterns in carotid artery plaques in patients and found that the initial entry of contrast agent into plaques correlated with the extent of neo-vascularization. The delivery of contrast agents into the

extravascular extracellular space appeared to depend on a combination of neo-vascular supply and permeability. Following ligand conjugation, low molecular weight gadolinium-based contrast agents are also suited for target-specific MR imaging of very abundant targets (31). However, due to possible higher accumulation in non-TCFA lesions, one should wait long enough after contrast agent administration for the washout of unbound contrast material.

3. CONCLUSIONS

Vascular endothelium in atherosclerotic plaques is known to be more permeable than healthy vessel wall endothelium. In this study three differently sized contrast agents were employed to study their ability to produce T_1-weighted MRI contrast enhancement, in non-TCFA and TCFA murine carotid atherosclerotic plaques at two stages of development. Blood flow through the lesioned artery after cast implantation was preserved, implying that the contrast agents were able to access the desired area. The two smallest of the tested contrast agents, i.e. micelles and Gd-HP-DO3A, resulted in contrast enhancement in all plaque phenotypes on T_1-weighted MR images. The maximum enhancement for Gd-HP-DO3A and micelles was shown to be dependent on contrast agent size and blood kinetics, which underscores that care must be exerted in interpreting plaque enhancement with targeted agents. Liposomes, on the other hand, were too large to permeate the vessel wall and caused no significant contrast enhancement in the atherosclerotic plaques. Confocal microscopy confirmed these findings. Histology showed that phenotype differences as well as sizes of the plaques were larger at 9 weeks after cast placement than at 6 weeks after cast placement.

These results imply that, when suitably modified with targeting ligands, the fast permeation of Gd-HP-DO3A into plaques makes low molecular weight contrast agents suitable for imaging of abundant targets inside atherosclerotic plaques. The lack of intraplaque accumulation of liposomes makes these particles a good candidate for imaging of plaque associated vascular markers, because these contrast materials cause little background enhancement and the endothelial markers are directly accessible from the vessel lumen. Micelles accumulate into atherosclerotic plaques on a longer timescale, which makes them suitable for imaging of less abundant markers inside atherosclerotic plaques. With this knowledge improvements can be made to the contrast agents for the detection of endothelial markers such as VCAM-1 (17) or intraplaque macrophages (27) and neovascularization (21).

4. EXPERIMENTAL

4.1. Preparation of paramagnetic liposomes and micelles

Liposomes and micelles were prepared by lipid film hydration (32). A mixture of the appropriate amounts of lipids was dissolved in chloroform:methanol 3:1 (v/v) and evaporated to dryness by rotary evaporation. For liposomes, Gd-DTPA-BSA [Gd-DTPA-bis(stearylamide)], DSPC (1,2-distearoyl-sn-glycero-3-phosphocholine), cholesterol and PEG2000-DSPE [1,2-distearoyl-sn-glycero-3-phosphoethanolamine-*N*-methoxy(polyethyleneglycol)2000] were used at a molar ratio of 0.75:1.1:1:0.15. For fluorescent detection, 0.1 mol% NIR664-DSPE (SyMO-Chem B.V., Eindhoven, The Netherlands) was added. For micelles, Gd-DTPA-BSA and PEG2000-DSPE were used at a molar ratio of 1:1 with 1% NIR664-DSPE. The lipid film was subsequently hydrated in HEPES buffered saline (HBS), containing 20 mM HEPES and 135 mM NaCl (pH 7.4). The liposomes were sized at 65°C using a Lipofast Extruder (Avestin, Canada) and a filter with a diameter of 100 nm. Micelles were prepared via lipid hydration and vigorous stirring at 65°C for 45 min. The size and size distribution were assessed by dynamic light scattering at 25°C with a Malvern ZetaSizer Nano S (Malvern, UK). The relaxivity was measured at 37°C and 1.41 T using a Minispec MQ60 Spectrometer (Bruker, Germany), and at room temperature and 6.3 T as described previously (33–35). The phospholipid concentration was determined by phosphate analysis according to Rouser (36) after destruction in perchloric acid.

4.2. Circulation half-lives and organ distribution of the contrast agents

The local institutional animal care and use committee approved all experimental procedures and the investigation conforms to the *Guide for the Care and Use of Laboratory Animals* (NIH publication no. 85–23, revised 1996). For the determination of the blood circulation half-lives of the different contrast agents, 12 female apoE$^{-/-}$ mice (age 12 weeks) that were on a Western-type diet (0.21% cholesterol) for a period of 12 weeks were anesthetized. Before contrast agent injection a 20 μl blood sample was obtained from the saphenous vein. Paramagnetic liposomes, micelles or Gd-HP-DO3A (ProHance, Bracco Diagnostics, Inc.) were injected via the tail vein (equivalent to 50 μmol Gd/kg body weight) and 20 μl blood samples were collected after 2, 15, 30, 45 and 60 min while the mouse was kept under anesthesia. Additional blood samples were obtained at 4, 8, 24 and 48 h after injection of the contrast agent. To prevent coagulation of the blood samples they were mixed with 20 μl of heparinized physiological salt solution (50 i.E. heparin/ml). After the last time point the mice were sacrificed by exsanguination and arterial PBS perfusion was performed. The liver, lungs, kidneys and spleen were excised, snap frozen and stored at −80 °C. The longitudinal relaxation rate (R_1) of the blood samples was determined at room temperature with a 6.3 T horizontal-bore scanner (Bruker BioSpin, Ettlingen, Germany) using a fast inversion recovery segmented FLASH sequence ($TE = 1.5$ ms, $TR = 3$ ms, flip angle = 15°, TI ranging from 67 to 4800 ms in 80 steps, overall repetition time = 20 s, FOV = 3×2.81 cm^2, matrix = 128×128, slice thickness = 1 mm, average = 2, total scan time = 21 min 20 s). The decrease in R_1 (ΔR_1) values of the blood samples over time were fitted in Origin (OriginLab Corporation, Northampton, USA) with a mono-exponential decay function ($y = Ae^{-t/\tau}$) to determine circulation half-lives ($t_{1/2} = \tau \ln 2$). Gadolinium content of liver, lung, kidney and spleen of one mouse of each group was determined with ICP-AES or ICP-MS (Philips Research, Eindhoven, The Netherlands).

4.3. Mouse model

For this study 36 female apoE$^{-/-}$ mice (age 12 weeks) were fed a Western-type diet (0.21% cholesterol) for a period of 3 weeks, after which a tapered cast was surgically placed around the right carotid artery (2). The stiff tapered cast (Promolding BV., The Hague, The Netherlands) with an inner diameter ranging from 500 μm upstream to 250 μm downstream was placed around the

right common carotid artery at least 1 mm upstream from the bifurcation. After cast placement a period of either 6 weeks or 9 weeks with continuing diet was allowed for plaque development.

4.4. In vivo MRI

MRI measurements were performed with a 6.3 T horizontal-bore animal scanner (Bruker BioSpin, Ettlingen, Germany) equipped with a 3 cm-diameter quadrature birdcage RF coil (Rapid Biomedical, Rimpar, Germany). The mice were initially anesthetized with 3% isoflurane in medical air, and kept on 1–2% isoflurane during the MRI experiments. The mice were placed in a custom-made cradle, which was kept at a constant temperature of approximately 37°C to maintain body temperature. Respiration was monitored with a balloon sensor connected to an ECG/respiratory unit (Rapid Biomedical, Rimpar, Germany).

The MRI protocol started with a 3D time-of-flight (TOF) gradient echo sequence of the neck area ($TR = 15$ ms, $TE = 2.5$ ms, $\alpha = 20°$, FOV $= 3.3 \times 3.5 \times 4\,cm^3$, matrix $= 256 \times 192 \times 192$, NEX $= 1$, scan time $= 9$ min). For contrast-enhanced imaging the mice were injected with paramagnetic liposomes, paramagnetic micelles or Gd-HP-DO3A ($n = 6$ for each group, yielding a total of 36 animals) through a catheter placed in the tail vein. T_1-weighted multi-slice spin-echo images ($TR = 800$ ms, $TE = 10.3$ ms, FOV $= 2.56 \times 2.56\,cm^2$, matrix $= 256 \times 256$, slice thickness $= 0.5$ mm, NEX $= 8$, scan time $= 27$ min) were acquired before and at different timepoints after contrast agent injection. Black blood was achieved by placing two saturation slabs below and above the neck region saturating inflowing blood. Slices were carefully positioned perpendicular to the right carotid artery both directly upstream and downstream of the cast by making a sagittal T_1-weighted image first (Fig. 3C). T_1-weighted images were acquired 15 min, 60 min and 24 h after injection of liposomes and micelles. Upon administration of Gd-HP-DO3A, mice were scanned up to 1 hour after injection with a higher temporal resolution by reducing the number of averages to 2 (scan time = 6.5 min) and again after 24 h. After the MRI experiments the mice were sacrificed by exsanguination followed by arterial PBS perfusion. The carotid arteries were dissected, embedded in 10% gelatin, snap frozen and stored at −80°C until further processing for histological evaluation.

4.5. Image analysis

For quantification of the vessel wall contrast levels, slices directly upstream and downstream of the cast were analyzed. Initially, the images were zero-filled to an in-plane pixel dimension of $50 \times 50\,\mu m^2$. Regions of interest (ROI) containing tissue directly surrounding the vessel lumen were drawn in Mathematica (Wolfram Research Inc.) for the left and right carotid arteries and the average signal intensities were calculated (I_W). ROIs were also drawn in surrounding muscle tissue (longus capitis muscle) and outside each mouse to calculate muscle tissue signal intensity (I_M) and noise level (I_N), respectively (inset of Fig. 3D). The percentage signal enhancement (%SE) was determined according to

$$\%SE = \left(\frac{I_{W,t}}{I_{W,pre}} - 1\right) \times 100\%$$

For comparison with data collected 24 h after contrast agent injection, the vessel wall signal intensities were normalized to muscle tissue. The resulting normalized percentage signal enhancement (%NSE) was determined according to

$$\%NSE = \left(\frac{I_{W,t}/I_{M,t}}{I_{W,pre}/I_{M,pre}} - 1\right) \times 100\%$$

4.6. Histology and fluorescence microscopy

Both the upstream and downstream plaques were cut into 8 μm-thick serial sections perpendicular to the vessel direction. Sections were stained with hematoxylin and eosin, Oil red O for lipids and picrosirius red for collagen (analyzed with a circular polarizing filter) at 80 μm intervals. Macrophages were detected by FITC labeled antibodies directed against CD68-FITC [dilution 1:100 (10 μg/ml), AbD Serotec, clone FA11], smooth muscle cells using FITC labeled antibodies directed against α-Smooth Muscle Actin-FITC (dilution 1:250, Sigma-Aldrich Inc., St Louis, MO, USA; clone 1A4) and the endothelium using antibodies directed against PECAM-1 [dilution 1:250 (2 μg/ml), BD Pharmingen, clone MEC13.3] with goat-anti rat IgG AlexaFluor 488 as secondary antibody [dilution 1:500 (4 μg/ml), Molecular Probe, Inc., Eugene, USA].

Bright-field microscopy was performed with a Zeiss Axio Observer Z1 microscope (Carl Zeiss, Inc.). Fluorescently labeled sections were analyzed by a Zeiss Axiovert 200M microscope (Carl Zeiss, Inc.). Macrophages, smooth muscle cells and the endothelium were visualized on separate sections with a 455–495 nm excitation and a 500–550 nm emission filter.

For detection of liposome and micelle fluorescence, confocal laser scanning microscopy was performed on a Zeiss LSM 510 META system (Carl Zeiss, Inc.). NIR664 was excited with a 633 nm HeNe laser. Emission was filtered through a band-pass filter of 650–710 nm. FITC or Alexa Fluor 488 was excited with a 488 nm argon laser in combination with an emission band-pass filter of 500–550 nm. Autofluorescence of elastin was excited with a 543 nm HeNe laser and emission was filtered through a bandpass filter of 565–615 nm.

4.7. Statistics

Statistical analyses were performed to test whether (1) %SE and %NSE had changed significantly upon injection of contrast agent in time, (2) contrast enhancement differed between contrast agents, and (3) the upstream and downstream plaques showed a distinct response. For this purpose, one-way analysis of variance (ANOVA; significance level $p < 0.05$) with Bonferroni correction for multiple comparisons was performed with Statgraphics Centurion XV (StatPoint Inc., Virginia, USA). Two-way ANOVA (significance level $p < 0.05$) was performed on the high-resolution vessel wall enhancement data after Gd-HP-DO3A injection to test whether %SE was significantly different for the TCFA lesion, non-TCFA lesion and the vessel wall of the left carotid artery.

Acknowledgements

This study was supported in part by the BSIK program entitled Molecular Imaging of Ischemic Heart Disease (project number BSIK03033) and by the EC-FP6-project DiMI, LSHB-CT-2005-512146, and was performed in the framework of the European Cooperation in the field of Scientific and Technical Research (COST) D38 Action Metal-Based Systems for Molecular Imaging Applications. Jo Habets and Leonie Niesen are acknowledged for

biotechnical assistance. Thea Haex and Jeannette Smulders are acknowledged for the ICP-AES and ICP-MS analysis.

REFERENCES

1. Pedersen EM, Oyre S, Agerbaek M, Kristensen IB, Ringgaard S, Boesiger P, Paaske WP. Distribution of early atherosclerotic lesions in the human abdominal aorta correlates with wall shear stresses measured in vivo. Eur J Vasc Endovasc Surg 1999; 18(4): 328–333.
2. Cheng C, Tempel D, van Haperen R, van der Baan A, Grosveld F, Daemen MJ, Krams R, de Crom R. Atherosclerotic lesion size and vulnerability are determined by patterns of fluid shear stress. Circulation 2006; 113(23): 2744–2753.
3. Virmani R, Burke AP, Farb A, Kolodgie FD. Pathology of the vulnerable plaque. J Am Coll Cardiol 2006; 47 (8 Suppl): C13–18.
4. Fayad ZA, Fallon JT, Shinnar M, Wehrli S, Dansky HM, Poon M, Badimon JJ, Charlton SA, Fisher EA, Breslow JL, Fuster V. Noninvasive in vivo high-resolution magnetic resonance imaging of atherosclerotic lesions in genetically engineered mice. Circulation 1998; 98(15): 1541–1547.
5. Choudhury RP, Aguinaldo JG, Rong JX, Kulak JL, Kulak AR, Reis ED, Fallon JT, Fuster V, Fisher EA, Fayad ZA. Atherosclerotic lesions in genetically modified mice quantified in vivo by non-invasive high-resolution magnetic resonance microscopy. Atherosclerosis 2002; 162(2): 315–321.
6. Hockings PD, Roberts T, Galloway GJ, Reid DG, Harris DA, Vidgeon-Hart M, Groot PH, Suckling KE, Benson GM. Repeated three-dimensional magnetic resonance imaging of atherosclerosis development in innominate arteries of low-density lipoprotein receptor–knockout mice. Circulation 2002; 106(13): 1716–1721.
7. Kampschulte A, Ferguson MS, Kerwin WS, Polissar NL, Chu B, Saam T, Hatsukami TS, Yuan C. Differentiation of intraplaque versus juxtaluminal hemorrhage/thrombus in advanced human carotid atherosclerotic lesions by in vivo magnetic resonance imaging. Circulation 2004; 110(20): 3239–3244.
8. Schneider JE, McAteer MA, Tyler DJ, Clarke K, Channon KM, Choudhury RP, Neubauer S. High-resolution, multicontrast three-dimensional-MRI characterizes atherosclerotic plaque composition in ApoE–/– mice ex vivo. J Magn Reson Imag 2004; 20(6): 981–989.
9. Sanz J, Fayad ZA. Imaging of atherosclerotic cardiovascular disease. Nature 2008; 451(7181): 953–957.
10. Saraste A, Nekolla SG, Schwaiger M. Cardiovascular molecular imaging: an overview. Cardiovasc Res 2009; 83(4): 643–652.
11. Barkhausen J, Ebert W, Heyer C, Debatin JF, Weinmann HJ. Detection of atherosclerotic plaque with Gadofluorine-enhanced magnetic resonance imaging. Circulation 2003; 108(5): 605–609.
12. Sirol M, Itskovich VV, Mani V, Aguinaldo JG, Fallon JT, Misselwitz B, Weinmann HJ, Fuster V, Toussaint JF, Fayad ZA. Lipid-rich atherosclerotic plaques detected by gadofluorine-enhanced in vivo magnetic resonance imaging. Circulation 2004; 109(23): 2890–2896.
13. Kerwin WS, O'Brien KD, Ferguson MS, Polissar N, Hatsukami TS, Yuan C. Inflammation in carotid atherosclerotic plaque: a dynamic contrast-enhanced MR imaging study. Radiology 2006; 241(2): 459–468.
14. Ruehm SG, Corot C, Vogt P, Kolb S, Debatin JF. Magnetic resonance imaging of atherosclerotic plaque with ultrasmall superparamagnetic particles of iron oxide in hyperlipidemic rabbits. Circulation 2001; 103(3): 415–422.
15. Trivedi RA, Mallawarachi C, JM UK-I, Graves MJ, Horsley J, Goddard MJ, Brown A, Wang L, Kirkpatrick PJ, Brown J, Gillard JH. Identifying inflamed carotid plaques using in vivo USPIO-enhanced MR imaging to label plaque macrophages. Arterioscler Thromb Vasc Biol 2006; 26(7): 1601–1606.
16. Trivedi RA, JM UK-I, Graves MJ, Cross JJ, Horsley J, Goddard MJ, Skepper JN, Quartey G, Warburton E, Joubert I, Wang L, Kirkpatrick PJ, Brown J, Gillard JH. In vivo detection of macrophages in human carotid atheroma: temporal dependence of ultrasmall superparamagnetic particles of iron oxide-enhanced MRI. Stroke 2004; 35(7): 1631–1635.
17. Nahrendorf M, Jaffer FA, Kelly KA, Sosnovik DE, Aikawa E, Libby P, Weissleder R. Noninvasive vascular cell adhesion molecule-1 imaging identifies inflammatory activation of cells in atherosclerosis. Circulation 2006; 114(14): 1504–1511.
18. Frias JC, Williams KJ, Fisher EA, Fayad ZA. Recombinant HDL-like nanoparticles: a specific contrast agent for MRI of atherosclerotic plaques. J Am Chem Soc 2004; 126(50): 16316–16317.
19. Amirbekian V, Lipinski MJ, Briley-Saebo KC, Amirbekian S, Aguinaldo JG, Weinreb DB, Vucic E, Frias JC, Hyafil F, Mani V, Fisher EA, Fayad ZA. Detecting and assessing macrophages in vivo to evaluate atherosclerosis noninvasively using molecular MRI. Proc Natl Acad Sci USA 2007; 104(3): 961–966.
20. Winter PM, Morawski AM, Caruthers SD, Fuhrhop RW, Zhang H, Williams TA, Allen JS, Lacy EK, Robertson JD, Lanza GM, Wickline SA. Molecular imaging of angiogenesis in early-stage atherosclerosis with $\alpha v\beta 3$-integrin-targeted nanoparticles. Circulation 2003; 108(18): 2270–2274.
21. Winter PM, Neubauer AM, Caruthers SD, Harris TD, Robertson JD, Williams TA, Schmieder AH, Hu G, Allen JS, Lacy EK, Zhang H, Wickline SA, Lanza GM. Endothelial $\alpha v\beta 3$ integrin-targeted fumagillin nanoparticles inhibit angiogenesis in atherosclerosis. Arterioscler Thromb Vasc Biol 2006; 26(9): 2103–2109.
22. Flacke S, Fischer S, Scott MJ, Fuhrhop RJ, Allen JS, McLean M, Winter P, Sicard GA, Gaffney PJ, Wickline SA, Lanza GM. Novel MRI contrast agent for molecular imaging of fibrin: implications for detecting vulnerable plaques. Circulation 2001; 104(11): 1280–1285.
23. Sirol M, Aguinaldo JG, Graham PB, Weisskoff R, Lauffer R, Mizsei G, Chereshnev I, Fallon JT, Reis E, Fuster V, Toussaint JF, Fayad ZA. Fibrin-targeted contrast agent for improvement of in vivo acute thrombus detection with magnetic resonance imaging. Atherosclerosis 2005; 182(1): 79–85.
24. Mulder WJ, Douma K, Koning GA, van Zandvoort MA, Lutgens E, Daemen MJ, Nicolay K, Strijkers GJ. Liposome-enhanced MRI of neointimal lesions in the ApoE-KO mouse. Magn Reson Med 2006; 55(5): 1170–1174.
25. van Bochove GS, Straathof R, Krams R, Nicolay K, Strijkers GJ. MRI-determined carotid artery flow velocities and wall shear stress in a mouse model of vulnerable and stable atherosclerotic plaque. Magn Reson Mater Phys 2010; 23(2): 77–84.
26. von der Thusen JH, van Berkel TJ, Biessen EA. Induction of rapid atherogenesis by perivascular carotid collar placement in apolipoprotein E-deficient and low-density lipoprotein receptor-deficient mice. Circulation 2001; 103(8): 1164–1170.
27. Mulder WJ, Strijkers GJ, Briley-Saboe KC, Frias JC, Aguinaldo JG, Vucic E, Amirbekian V, Tang C, Chin PT, Nicolay K, Fayad ZA. Molecular imaging of macrophages in atherosclerotic plaques using bimodal PEG-micelles. Magn Reson Med 2007; 58(6): 1164–1170.
28. Briley-Saebo KC, Shaw PX, Mulder WJ, Choi SH, Vucic E, Aguinaldo JG, Witztum JL, Fuster V, Tsimikas S, Fayad ZA. Targeted molecular probes for imaging atherosclerotic lesions with magnetic resonance using antibodies that recognize oxidation-specific epitopes. Circulation 2008; 117(25): 3206–3215.
29. Yuan C, Kerwin WS, Ferguson MS, Polissar N, Zhang S, Cai J, Hatsukami TS. Contrast-enhanced high resolution MRI for atherosclerotic carotid artery tissue characterization. J Magn Reson Imag 2002; 15(1): 62–67.
30. Wasserman BA, Smith WI, Trout HH 3rd, Cannon RO 3rd, Balaban RS, Arai AE. Carotid artery atherosclerosis: in vivo morphologic characterization with gadolinium-enhanced double-oblique MR imaging initial results. Radiology 2002; 223(2): 566–573.
31. Burtea C, Laurent S, Murariu O, Rattat D, Toubeau G, Verbruggen A, Vanszthertem D, Vander Elst L, Muller RN. Molecular imaging of alpha v beta3 integrin expression in atherosclerotic plaques with a mimetic of RGD peptide grafted to Gd-DTPA. Cardiovasc Res 2008; 78(1): 148–157.
32. Mulder WJ, Strijkers GJ, Griffioen AW, van Bloois L, Molema G, Storm G, Koning GA, Nicolay K. A liposomal system for contrast-enhanced magnetic resonance imaging of molecular targets. Bioconjug Chem 2004; 15(4): 799–806.
33. van Tilborg GA, Geelen T, Duimel H, Bomans PH, Frederik PM, Sanders HM, Deckers NM, Deckers R, Reutelingsperger CP, Strijkers GJ, Nicolay K. Internalization of annexin A5-functionalized iron oxide particles by apoptotic Jurkat cells. Contrast Media Mol Imag 2009; 4(1): 24–32.

34. Sanders HM, Strijkers GJ, Mulder WJ, Huinink HP, Erich SJ, Adan OC, Sommerdijk NA, Merkx M, Nicolay K. Morphology, binding behavior and MR-properties of paramagnetic collagen-binding liposomes. Contrast Media Mol Imag 2009; 4(2): 81–88.
35. Hak S, Sanders HM, Agrawal P, Langereis S, Grull H, Keizer HM, Arena F, Terreno E, Strijkers GJ, Nicolay K. A high relaxivity Gd(III)DOTA-DSPE-based liposomal contrast agent for magnetic resonance imaging. Eur J Pharm Biopharm 2009; 72(2): 397–404.
36. Rouser G, Fkeischer S, Yamamoto A. Two dimensional thin layer chromatographic separation of polar lipids and determination of phospholipids by phosphorus analysis of spots. Lipids 1970; 5(5): 494–496.

